Compander Design for OFDM PAPR Reduction Using Optimal Perturbation of Piecewise Linear Segments

Stephen P. DelMarco, *Member, IEEE*

***Abstract*—In this paper, we develop an optimal perturbation approach to design companders to mitigate the peak-to-average power ratio problem experienced by orthogonal frequency division multiplexing (OFDM) signals. Specifically, we generalize single-linear component design approaches, which modify the Rayleigh–distributed OFDM signal amplitude tail, to use of multiple contiguous piecewise linear components. The new compander design approach defines and solves a constrained optimization problem to optimally perturb a given proposed multicomponent piecewise linear segment set to meet the power and probability density function constraints. The use of multiple piecewise linear components provides greater design flexibility to meet the constraints, thus providing solutions for pairs of inflection points and cutoff values where more rigidly designed companders fail to exist. We present examples of compander design, and demonstrate compander performance through numerical simulation. The new compander design approach can generate companders that offer performance improvements over current companders.**

***Index Terms*—Nonlinear companding transform, orthogonal frequency division multiplexing (OFDM), peak-to-average power ratio (PAPR).**

I. Introduction

COMPANDING techniques have proven their use in reducing the large peak-to-average power ratio (PAPR) that occurs in orthogonal frequency division multiplexing (OFDM) signals. Large PAPR results from constructive interference among the OFDM sub-carriers, which accounts for the long tail of the Rayleigh-distributed amplitude values, and can drive the signal amplitude into the power amplifier saturation region.

Companders typically apply a weighting function to the OFDM signal amplitude to decrease the probability of large amplitudes. This amplitude downweighting limits amplifier saturation and reduces the demodulation performance degradation that would otherwise occur if no PAPR reduction technique were used. Companders usually upweight a lower-probability amplitude range, to maintain average power and mitigate deleterious effects on demodulation performance resulting from the amplitude value modification.

Manuscript received August 9, 2017; revised November 14, 2017; accepted November 20, 2017.

The author is with Technology Solutions, BAE Systems, Burlington, MA 01803 USA (e-mail: stephen.delmarco@baesystems.com).

Color versions of one or more of the figures in this paper are available online at http://ieeexplore.ieee.org.

Digital Object Identifier 10.1109/TBC.2017.2781129

Companders generally provide low-complexity solutions for PAPR reduction. Other effective, but high complexity, approaches have been developed for PAPR reduction, and work continues toward reducing computational complexity of these approaches. To reduce computational complexity of Partial Transmit Sequences (PTS), suboptimal heuristic approaches have been developed [1] using elements of chaos theory with biomimetic natural selection techniques to choose PTS sequences. Reduced complexity PTS approaches have been developed by exploiting dominant time-domain samples from alternative OFDM signals to efficiently estimate PAPR. New, more efficient metrics for time-domain sample selection, providing more accurate PAPR estimation, have been developed [2] which reduce complexity. Additionally, PTS approaches typically require transmission of side information. Approaches have been developed that eliminate the need for side-information transmission by embedding the side information directly into the signal [3]. Kim [4] develops a cyclic shifted sequences scheme for PTS, which replaces the rotation factor multiplication by circulant signal shifts, and provides criteria for efficiently choosing shift sets that reduce PAPR.

Suboptimal approximations have been made to Tone Injection approaches to reduce computational complexity. Wang *et al.* [5] define a complex constellation perturbation optimization problem to find constellation perturbations that minimize clipping distortion. They decouple the optimization problem into a pair of lower-dimensional optimizations over real and imaginary parts. Simulations reveal that the optimal constellation perturbations are highly dependent on the signs of the real and imaginary parts of the clipping distortion, which they exploit to reduce the perturbation search space. Hou *et al.* [6] reduce the number of fast Fourier transforms (FFTs), performed in the clipping noise optimization problem, to find the new, equivalent constellations.

For Tone Reservation approaches, Yu and Jin [7] reduce computational complexity by eliminating the Fourier transform operations, replacing them with a time-domain kernel matrix that is calculated once, offline.

Shu *et al.* [8] combine ideas from invertible subset low-density parity check (LDPC) codes, which give good PAPR reduction performance, with quasi-cyclic LDPC codes, which can be efficiently implemented, to obtain advantages of both approaches.

Computational efficiency is continually increasing for Active Constellation Extension (ACE) approaches. Wang *et al.* [9] perform subcarrier grouping which enables use of lower dimensional FFTs in the optimization scheme thereby reducing computational complexity. Liu *et al.* [10] provide a clipping approach in which clipped frequency domain signal points are migrated to the nearest constellation point by flipping bit values. Constellation extension, as measured by Euclidean distance, is replaced with a metric based on the number of flipped bits. Error correction coding is used to mitigate bit flipping effects on demodulation performance, and precludes the need for transmission of the flipped-bits side information.

In pre-coding approaches, Wang *et al.* [11] develop a new precoding matrix, which combines with the inverse Fourier transform matrix, using Gaussian integer sequences. The resulting product matrix contains fewer non-zero entries thus reducing computational complexity.

New trends in PAPR reduction techniques include application of machine learning and compressed sensing approaches. Neural net techniques have been used to reduce computation of ACE [12] and clipping and filtering approaches [13]. Compressed sensing [14] is used to more accurately reconstruct clipping noise, for later cancellation at the receiver, by mitigating channel effects in a clipping and filtering scheme.

Current trends in compander development include the development of hybrid approaches that combine companding with ACE [15], Selective Mapping [16], and PTS [17]. Hybrid precoding techniques have been developed that use the Hadamard transform [18]–[20], Discrete Fourier Transform [21], Hartley transform [22], [23] or subcarrier shaping [24]. Iterative approaches have been developed that work with companding to reduce out-of-band interference through frequency-domain filtering [25].

Also, traditional classic companders, such as the μ-law and A-law companders [26]–[29] that were originally adapted from speech processing, have recently been improved. Improved companding performance results from modifying the functional form of the companding curve across different amplitude range segments [30] or adapting parameter values [31].

Companders can be designed by direct amplitude weighting considerations or by exploiting statistical properties of the OFDM signal. One successful statistical exploitation approach to compander design modifies the Rayleigh amplitude distribution to re-distribute probability from the long Rayleigh tail, to an amplitude region below a cutoff value [32]–[41].

This probability redistribution preserves average signal power and satisfies the probability density function (p.d.f.) constraints; non-negativity of the p.d.f., and unit value for the maximum of the cumulative distribution function (c.d.f.) - the unity c.d.f. constraint. This probability re-distribution approach eliminates large amplitude values, thus reducing PAPR, but introduces signal distortion which can reduce demodulation performance relative to uncompanded and unsaturated signals.

Among the Rayleigh distribution transformation design techniques, use of a single linear segment to modify the Rayleigh distribution tail has shown high performance [32], [33]. Such an approach leaves much of the original amplitude distribution unchanged, which helps to mitigate demodulation errors.

However, as shown in Section II, single component approaches can fail to exist for certain pairs of inflection and cutoff points. These fail because too much area under the single linear component curve causes the modified p.d.f. to integrate to a value larger than unity value. In these cases, multi-component approaches provide additional design flexibility which can restore the unity c.d.f. condition.

In this paper, we present a compander design approach which modifies the Rayleigh distribution tail using multiple contiguous piecewise linear segments. We assume, as given, a proposed set of contiguous piecewise linear components meant to modify the tail of the Rayleigh amplitude distribution for compander design. We find a minimal perturbation that satisfies the unity c.d.f, constant power, and p.d.f. non-negativity constraints.

We solve this problem using a constrained optimization approach via Lagrange multipliers. We determine perturbation values on the ordinates of the linear components that minimally perturb the components while simultaneously providing a solution that meets the constraints. Through simulation we demonstrate performance of the new companders.

This paper serves two purposes. First, it extends the single linear segment compander approach to multiple contiguous linear segments. Second, it solves a problem raised during compander development in our prior work [42]. There, we developed a compander by defining and solving a constrained optimization problem. We found the piecewise linear function that optimally approximates the Rayleigh p.d.f. up to the cutoff value. However, solutions could be negative over a small range $[0, \varepsilon)$, thus violating the non-negativity constraint on probability density functions. To fix this negativity problem, we default to the Rayleigh p.d.f. over $[0, \varepsilon)$, and minimally perturb the tail of the approximation p.d.f. to meet the unity c.d.f. and constant power constraints. The technique presented in this paper provides the mechanism for perturbing the tail of the approximating p.d.f.

The rest of this paper is organized as follows. Section II justifies the multi-component approach by providing conditions under which the single-component solution fails to exist. Section III defines and solves the constrained optimization problem. Section IV presents simulation results and Section V presents concluding remarks.

II. Limitations of Single-Linear Component Solutions

In this section we show how single-linear component solutions can fail to exist for certain combinations of inflection and cutoff values. Assume a linear component is defined over interval $[A_I, A_C]$ for inflection point A_I and cutoff value A_C. Denote the associated ordinates by β_I, β_C. The linear component is given by $y = mx + b$ where

$$m = \frac{\beta_C - \beta_I}{A_C - A_I}, \quad b = \beta_I - \frac{A_I(\beta_C - \beta_I)}{A_C - A_I}$$

and $\beta_I = f_R(A_I)$, $\beta_C = f_R(A_C) \geq 0$. For Rayleigh distribution

$$f_R(x) = \frac{2x}{\sigma^2} e^{-\frac{x^2}{\sigma^2}}$$

the unity c.d.f. condition becomes (see Figure 1)

$$\int_0^{A_I} f_R(x)dx + \int_{A_I}^{A_C} (mx+b)dx = 1.$$

Performing the integration and simplifying produces

$$\beta_C = \left[\frac{2e^{-\frac{A_I^2}{\sigma^2}}}{\sigma^2(A_C - A_I)}\right]\left[\sigma^2 - A_I(A_C - A_I)\right]$$

which can only be negative if

$$\frac{\sigma^2}{A_I} < A_C - A_I$$

in which case the linear component fails to meet the unity c.d.f constraint. As an example, for $\sigma^2 = 1$, $A_I = 1$, then the constraint fails for $A_C > 2.0$.

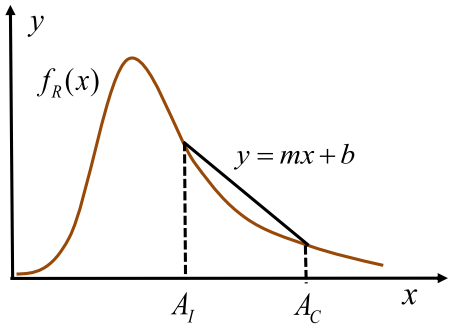

Fig. 1. For certain pairs of inflection and cutoff amplitude values, the integral under the linear component can become too large to satisfy the unity c.d.f. constraint.

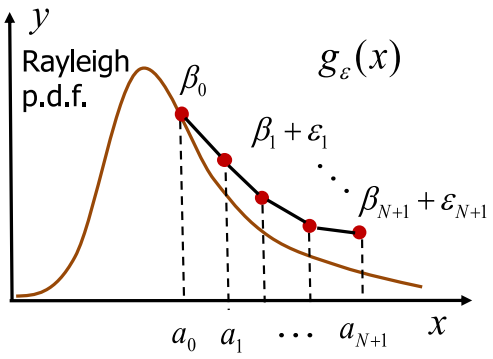

Fig. 2. Perturbed function designed to restore constraints.

III. Compander Design Using Minimal Perturbation

This section formulates the constrained, minimal perturbation problem and presents the solution.

A. Constrained Minimal Perturbation Problem

Assume a baseline set of piecewise linear components is given. Assume these are characterized by abscissa breakpoints $(a_0, \ldots, a_{N+1})$, $a_0 > 0$, which partition the interval $[A_I, A_C]$ with $a_0 = A_I$, $a_{N+1} = A_C$ and corresponding positive ordinate values $(\beta_0, \ldots, \beta_{N+1})$. These components are meant to modify the tail of the Rayleigh amplitude distribution, but do not necessarily satisfy the unity c.d.f. and constant power constraints. Therefore, we look for a perturbation set of ordinate values that restore the unity c.d.f. and constant power constraints, as shown in Figure 2.

Define a perturbed function

$$g_\varepsilon(x) = \sum_{i=0}^{N} U_i(x, \varepsilon_i, \varepsilon_{i+1}) \tag{1}$$

where the $U_i(x, \varepsilon_i, \varepsilon_{i+1})$ are perturbed, compactly-supported linear segments

$$U_i(x, \varepsilon_i, \varepsilon_{i+1}) = \begin{cases} \left(\frac{(\beta_{i+1}+\varepsilon_{i+1})-(\beta_i+\varepsilon_i)}{a_{i+1}-a_i}\right)(x - a_i) + (\beta_i + \varepsilon_i) & \text{for } x \in [a_i, a_{i+1}] \\ 0 & \text{otherwise} \end{cases} \tag{2}$$

for $0 \leq i \leq N$. Take $\varepsilon_0 = 0$ so that $(a_0, \beta_0 + \varepsilon_0) = (a_0, \beta_0)$ thus leaving the first point fixed and maintaining a continuous function.

B. Constraints

The unity c.d.f. constraint imposes conditions, derived in Appendix A, on the perturbation parameters. These conditions are

$$\sum_{i=0}^{N} \xi_i \varepsilon_i + \xi_i \varepsilon_{i+1} = C_1 \tag{3}$$

for values of ξ_i, C_1 defined in Appendix A.

Similarly, the constant power constraint on $g_\varepsilon(x)$ induces constraints on the perturbation parameters, as shown in Appendix B. These constraints are

$$\sum_{i=0}^{N} \eta_i^1 \varepsilon_i + \eta_i^2 \varepsilon_{i+1} = C_2 \tag{4}$$

for values of η_i^1, η_i^2, C_2 given in Appendix B.

It often happens that the optimal solution automatically satisfies the p.d.f. non-negativity constraint, so to simplify the solution we forgo explicit consideration of this constraint.

C. Optimal Perturbation Parameters

To find the minimal perturbation $g_\varepsilon(x)$ away from $g(x)$, choose parameters $(\varepsilon_1, \ldots, \varepsilon_{N+1})$ to minimize

$$F_\varepsilon(\varepsilon_1, \ldots, \varepsilon_{N+1}) = \sum_{i=1}^{N+1} \varepsilon_i^2. \tag{5}$$

Rearranging terms in (3) and (4) and simplifying produces constraints

$$h_1(\varepsilon_1,\ldots,\varepsilon_{N+1}) = C_1,$$
$$h_2(\varepsilon_1,\ldots,\varepsilon_{N+1}) = C_2$$

for constraint functions

$$h_1(\varepsilon_1,\ldots,\varepsilon_{N+1}) = \left(\sum_{i=1}^{N-1}(\xi_{i-1}+\xi_i)\varepsilon_i\right) + (\xi_{N-1}+\xi_N)\varepsilon_N + \xi_N\varepsilon_{N+1} \quad (6)$$

$$h_2(\varepsilon_1,\ldots,\varepsilon_{N+1}) = \left(\sum_{i=1}^{N-1}\left(\eta_{i-1}^2+\eta_i^1\right)\varepsilon_i\right) + \left(\eta_{N-1}^2+\eta_N^1\right)\varepsilon_N + \eta_N^2\varepsilon_{N+1}. \quad (7)$$

The Lagrangian is given by

$$\Lambda_h(\varepsilon_1,\ldots,\varepsilon_{N+1},\lambda_1,\lambda_2) = F_\varepsilon(\varepsilon_1,\ldots,\varepsilon_{N+1}) + \lambda_1\left[h_1(\varepsilon_1,\ldots,\varepsilon_{N+1}) - C_1\right] + \lambda_2\left[h_2(\varepsilon_1,\ldots,\varepsilon_{N+1}) - C_2\right]$$

and the critical point is found by simultaneously solving the set of equations

$$\frac{\partial\Lambda_h}{\partial\varepsilon_j} = \frac{\partial F_\varepsilon}{\partial\varepsilon_j} + \lambda_1\frac{\partial h_1}{\partial\varepsilon_j} + \lambda_2\frac{\partial h_2}{\partial\varepsilon_j} = 0,$$
$$\frac{\partial\Lambda_h}{\partial\lambda_1} = h_1(\varepsilon_1,\ldots,\varepsilon_{N+1}) - C_1 = 0,$$
$$\frac{\partial\Lambda_h}{\partial\lambda_2} = h_2(\varepsilon_1,\ldots,\varepsilon_{N+1}) - C_2 = 0. \quad (8)$$

From (5), (6), and (7)

$$\frac{\partial\Lambda_h}{\partial\varepsilon_j} = \begin{cases} 2\varepsilon_i + \lambda_1(\xi_{i-1}+\xi_i) + \lambda_2\left(\eta_{i-1}^2+\eta_i^1\right) & \text{if } 1\le i\le N \\ 2\varepsilon_{N+1} + \lambda_1(\xi_N) + \lambda_2\left(\eta_N^2\right) & \text{if } i = N+1 \end{cases}.$$

To find $\varepsilon_i, \lambda_1, \lambda_2$, solve, numerically, the following system of equations:

$$\begin{pmatrix} (\xi_0+\xi_1) & \left(\eta_0^2+\eta_1^1\right) & 2 & 0 & & & 0 \\ (\xi_1+\xi_2) & \left(\eta_1^2+\eta_2^1\right) & 0 & 2 & 0 & & 0 \\ \vdots & & & & \ddots & & \\ & & & & & \ddots & \\ (\xi_{i-1}+\xi_i) & \left(\eta_{i-1}^2+\eta_i^1\right) & 0 & & 2 & 0 & 0 \\ \vdots & & & & & \ddots & \\ \xi_N & \eta_N^2 & 0 & & & 0 & 2 \\ 0 & 0 & (\xi_0+\xi_1) & \cdots & & (\xi_{N-1}+\xi_N) & \xi_N \\ 0 & 0 & \left(\eta_0^2+\eta_1^1\right) & \cdots & & \left(\eta_{N-1}^2+\eta_N^1\right) & \eta_N^2 \end{pmatrix} \times \begin{pmatrix} \lambda_1 \\ \lambda_2 \\ \\ \\ \varepsilon_i \\ \\ \\ \varepsilon_{N-1} \\ \varepsilon_N \\ \varepsilon_{N+1} \end{pmatrix} = \begin{pmatrix} 0 \\ 0 \\ \vdots \\ \\ \\ \vdots \\ \\ 0 \\ C_1 \\ C_2 \end{pmatrix}. \quad (9)$$

D. Verification of Minimum

The sign test on the sequence of principal minors of the Hessian of the Lagrangian determines the critical point type [43]. The Hessian is given as:

$$H = \begin{pmatrix} 0 & 0 & \frac{\partial h_1}{\partial\varepsilon_1} & \cdots & \frac{\partial h_1}{\partial\varepsilon_{N+1}} \\ 0 & 0 & \frac{\partial h_2}{\partial\varepsilon_1} & \cdots & \frac{\partial h_2}{\partial\varepsilon_{N+1}} \\ & & \ddots & & \\ & & \ddots & \frac{\partial^2 F}{\partial\varepsilon_j\partial\varepsilon_i} + \lambda_1\frac{\partial^2 h_1}{\partial\varepsilon_j\partial\varepsilon_i} + \lambda_2\frac{\partial^2 h_2}{\partial\varepsilon_j\partial\varepsilon_i} & \\ & & \ddots & & \end{pmatrix}.$$

We have

$$\frac{\partial^2 h_1}{\partial\varepsilon_i\partial\varepsilon_j} = \frac{\partial^2 h_2}{\partial\varepsilon_i\partial\varepsilon_j} = 0,$$
$$\frac{\partial^2 F_\varepsilon}{\partial\varepsilon_j^2} = 2,\ \frac{\partial^2 F_\varepsilon}{\partial\varepsilon_j\partial\varepsilon_k} = 0,\ k\ne j,$$
$$\frac{\partial h_1}{\partial\varepsilon_i} = \begin{cases} \xi_{i-1}+\xi_i & \text{if } 1\le i\le N \\ \xi_N & \text{if } i = N+1 \end{cases},$$
$$\frac{\partial h_2}{\partial\varepsilon_i} = \begin{cases} \eta_{i-1}^2+\eta_i^1 & \text{if } 1\le i\le N \\ \eta_N^2 & \text{if } i = N+1 \end{cases}.$$

or

$$H = \begin{pmatrix} 0 & 0 & \xi_0+\xi_1 & \cdots & \xi_{i-1}+\xi_i & \cdots & \xi_N \\ 0 & 0 & \eta_0^2+\eta_1^1 & \cdots & \eta_{i-1}^2+\eta_i^1 & \cdots & \eta_N^2 \\ & & 2 & & & & \\ & & & & & 0 & \\ & & & & \ddots & & \\ & & & & & & 2 \end{pmatrix}. \quad (10)$$

Numerical evaluation of the sign test shows that the critical point is a local minimum.

E. Compander and Decompander

The compander and decompander are derived in [42]. For input signal $x(n)$ and output companded signal $y(n)$, the compander is given as

$$y = \operatorname{sgn}(x)\sqrt{\frac{1-e^{-\frac{x^2}{\sigma^2}} - Z_{i-1}}{\gamma_i} - \left(\frac{\lambda_i}{\gamma_i} - \frac{\delta_i^2}{4\gamma_i^2}\right)} - \frac{\delta_i}{2\gamma_i},$$

for $a_i \le x < a_{i+1}$, $0 \le i < N$, and

$$\gamma_i = \frac{m_i}{2},\quad \delta_i = b_i,\quad \lambda_i = -\left(m_i\frac{a_i^2}{2} + b_i a_i\right),$$
$$m_i = \frac{\beta_{i+1}-\beta_i}{a_{i+1}-a_i},\quad b_i = \beta_i - \frac{a_i(\beta_{i+1}-\beta_i)}{a_{i+1}-a_i},$$
$$Z_i = Z_{i-1} + \frac{\beta_{i+1}(a_{i+1}-a_i) + \beta_i(a_{i+1}-a_i)}{2},$$
$$Z_{-1} = 1 - e^{-\frac{a_0^2}{\sigma^2}}.$$

TABLE I
PERTURBED FUNCTION BREAKPOINT VALUES (PERTURBED-1)

a_i	β_i Baseline	β_i Perturbed
1.0000	0.7350	0.7350
1.1246	0.6307	0.6167
1.2492	0.5418	0.5030
1.3738	0.4685	0.4023
1.4984	0.4107	0.3146
1.6229	0.3684	0.2397
1.7475	0.3416	0.1778
1.8721	0.3304	0.1288
1.9967	0.3347	0.0927
2.1213	0.3545	0.2194

The decompander is derived as

$$x = \mathrm{sgn}(y)\sqrt{-\sigma^2 \ln\left(-\gamma_i\left(y + \frac{\delta_i}{2\gamma_i}\right)^2 - \lambda_i + \frac{\delta_i^2}{4\gamma_i} + 1 - Z_{i-1}\right)}.$$

IV. NUMERICAL RESULTS

In this section we generate numerical simulation results demonstrating compander design and performance.

A. Numerical Solutions and Analysis

We provide three examples to illustrate compander design. In each example, an initial set of ten argument breakpoints, with corresponding ordinate values, are provided as a proposed compander shape. Three different inflection points are defined: $A_I \in \{1.2,\ 1.416,\ 1.7\}$ to range over the backside of the Rayleigh distribution. A cutoff value of $A_C = 2.1213$ was chosen, for comparison with the optimal compander from [42]. The argument breakpoint and ordinate values are shown in Tables I–III. These initial amplitude distribution tail modifications do not satisfy the unity p.d.f. and constant power constraints. In each case, we solve system (9) to determine the optimal perturbation parameters. Figures 3, 4, and 5 display the proposed baseline shape, the nominal Rayleigh distribution, and the minimal perturbed solution meeting the constraints. In each case, as designed, the perturbed solution modifies the ordinate values to satisfy the constraints.

Figure 6 displays the compander functions for each of the design examples. The companders in Figure 6 show the characteristic shape of companders which modify the Rayleigh distribution tail. The initial part of the compander, prior to the inflection point, leaves the signal amplitude value unchanged. Between the inflection point and cutoff point, the compander upweights amplitude values close to the inflection point and downweights values near the cutoff value to maintain the average power level.

B. Simulation Results

To demonstrate a design tradeoff provided by the proposed companders, we generate numerical performance results for QPSK-modulated OFDM signals. We use sixty four carriers, an additive white Gaussian noise channel model, and an oversampling factor of four to model the PAPR from continuous signals. We choose $\sigma = 1.0$ in the Rayleigh signal amplitude distribution to provide unit power signals. We use ten thousand random signal realizations for each noise level. We generate numerical symbol error rates to measure demodulation performance, the complimentary cumulative distribution function (CCDF) to quantify PAPR rejection performance, and power spectrums for evaluation of out-of-band power rejection.

TABLE II
PERTURBED FUNCTION BREAKPOINT VALUES (PERTURBED-2)

a_i	β_i Baseline	β_i Perturbed
1.4160	0.3801	0.3801
1.4944	0.3278	0.2687
1.5727	0.2848	0.2245
1.6511	0.2509	0.1895
1.7295	0.2262	0.1636
1.8078	0.2108	0.1469
1.8862	0.2046	0.1393
1.9646	0.2076	0.1409
2.0429	0.2198	0.1516
2.1213	0.2412	0.2066

TABLE III
PERTURBED FUNCTION BREAKPOINT VALUES (PERTURBED-3)

a_i	β_i Baseline	β_i Perturbed
1.7000	0.1884	0.1884
1.7468	0.1848	0.0193
1.7936	0.1834	0.0426
1.8404	0.1842	0.0687
1.8872	0.1872	0.0977
1.9341	0.1924	0.1295
1.9809	0.1998	0.1641
2.0277	0.2093	0.2016
2.0745	0.2211	0.2419
2.1213	0.2350	0.2552

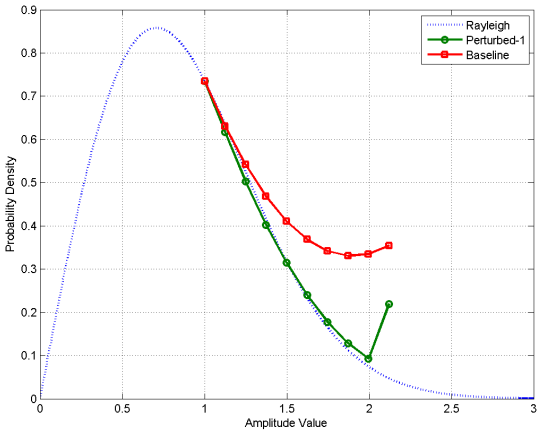

Fig. 3. Perturbed function (Perturbed-1) designed to restore constraints.

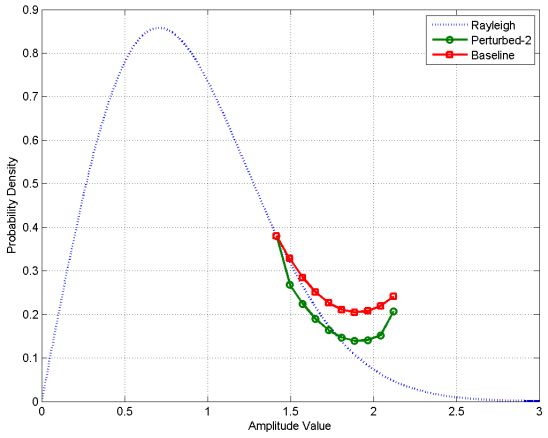

Fig. 4. Perturbed function (Perturbed-2) designed to restore constraints.

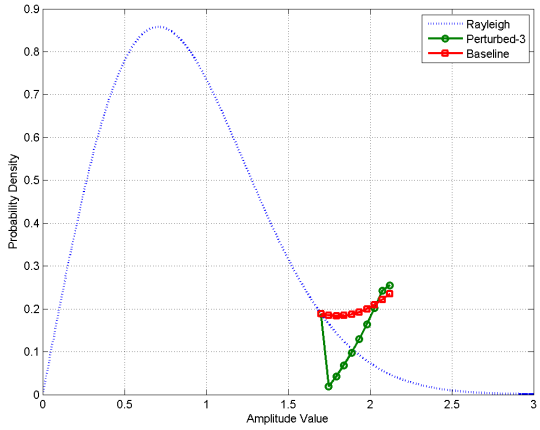

Fig. 5. Perturbed function (Perturbed-3) designed to restore constraints.

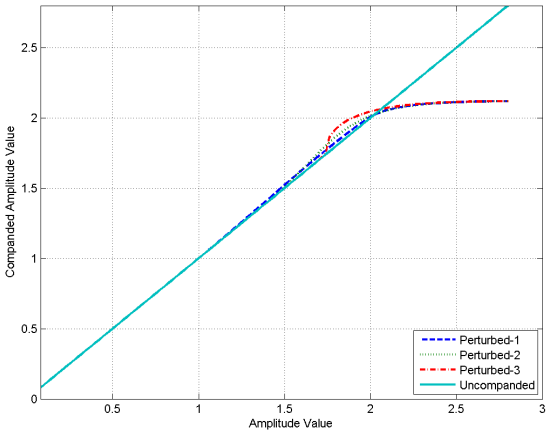

Fig. 6. Companding functions.

We generated performance results with use of the nonlinear, zero-phase power amplifier model used in [42] for high-, medium-, and low- saturation levels. Specifically, the output signal amplitude is given as

$$|y_{OUT}(t)| = \frac{a|y_{IN}(t)|}{\left[1 + \left(\frac{|y_{IN}(t)|}{A_{SAT}}\right)^{2p}\right]^{\frac{1}{2p}}}$$

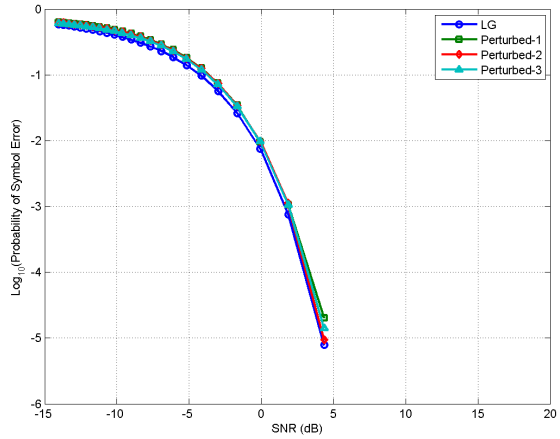

Fig. 7. Symbol error rate performance; low-level of power amplifier saturation.

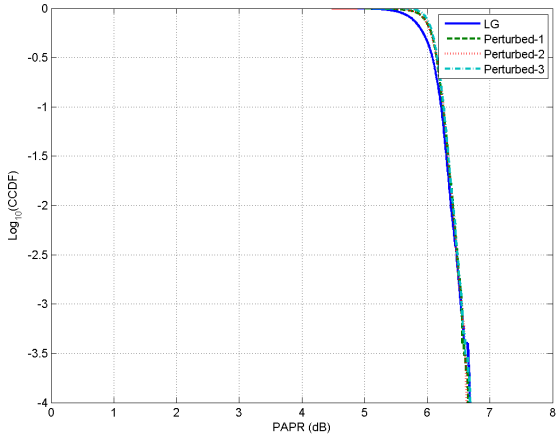

Fig. 8. PAPR reduction performance; low-level of power amplifier saturation.

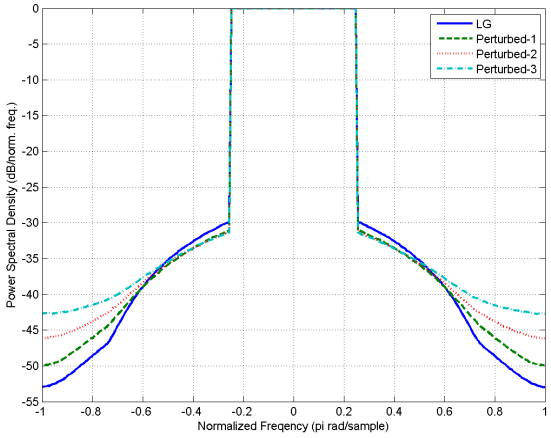

Fig. 9. Out-of-band power rejection; low-level of power amplifier saturation.

for input signal $y_{IN}(t)$, saturation values $A_{SAT} \in \{1.0, 2.0, 3.0\}$ where smaller values indicate higher levels of saturation, and nonlinearity parameter $p = 2$.

We compare performance against the optimal compander – called the LG compander developed in [42], which was demonstrated therein to provide performance advantages over current high-performance companders. We choose the same

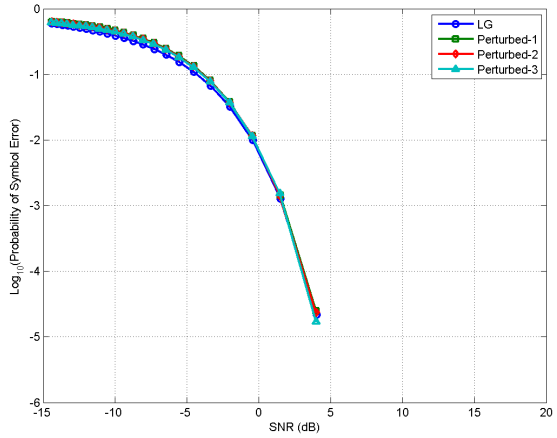

Fig. 10. Symbol error rate performance; medium-level of power amplifier saturation.

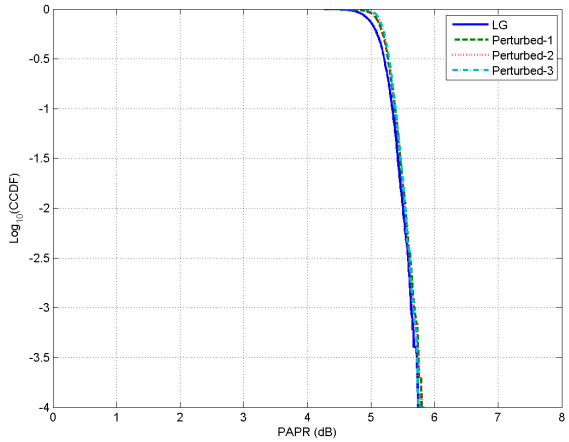

Fig. 11. PAPR reduction performance; medium-level of power amplifier saturation.

cutoff value, $A = 2.1213$. The argument breakpoints and corresponding ordinal values for the LG compander are:

$$a_i \in \{0.0055,\ 0.1818,\ 0.3581,\ 0.5345,\ 0.7108,\ 0.8871,\ 1.0634,\ 1.2397,\ 1.4160,\ 1.5924,\ 1.7687,\ 1.9450,\ 2.1213\},$$

$$\beta_i \in \{0.0001,\ 0.3449,\ 0.6283,\ 0.8045,\ 0.8602,\ 0.8105,\ 0.6899,\ 0.5385,\ 0.3903,\ 0.2668,\ 0.1764,\ 0.1182,\ 0.0857\}.$$

Relative to the LG compander the perturbed solution provides an out-of-band power rejection performance improvement, for adjacent frequency bins, for moderate power amplifier saturation levels. This performance improvement comes at the cost of a small performance degradation in demodulation performance.

Figures 7 and 8 show symbol error rate and PAPR rejection performance, respectively, for the low-level power amplifier saturation level. Figure 9 contains the power spectrum. Figures 7 and 8 show a small reduction in demodulation performance and PAPR rejection, while Figure 9 shows that the perturbed solution gives a maximum of more than 1.5 dB

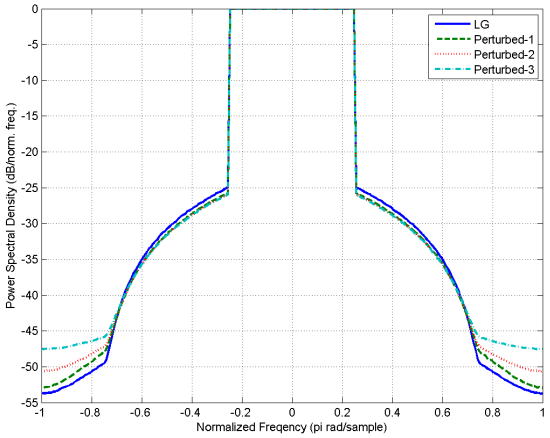

Fig. 12. Out-of-band power rejection; medium-level of power amplifier saturation.

TABLE IV
OUT-OF-BAND POWER REJECTION PERFORMANCE

Amplifier Saturation Level	**Performance Improvement (dB); Adjacent Bins**		
	Perturbed-1	Perturbed-2	Perturbed-3
Low	1.20	1.39	1.54
Medium	0.70	0.93	0.99
	Performance Degradation (dB); Boundary Bins		
Low	-2.95	-6.82	-10.28
Medium	-0.81	-3.14	-6.23

improvement in out-of-band power rejection for adjacent frequency bins.

For the medium-level power amplifier saturation, the perturbed solution gives even smaller demodulation and PAPR rejection performance degradations (Figures 10 and 11), while providing a maximum of almost 1.0 dB improvement in out-of-band power rejection for nearby frequency bins (Figure 12).

Table IV summarizes the out-of-band power rejection performance of the three perturbed solutions relative to the performance of the LG compander. As shown in Table IV, the perturbed solutions tradeoff power rejection performance between the adjacent and boundary frequency bins. The perturbed compander solutions therefore provide flexibility in compander design to meet various performance requirements.

V. CONCLUSION

In this paper, we provided an optimal perturbation approach to designing companders using multi-component, piecewise linear segments for modification of the signal amplitude distribution tail. For moderate power amplifier saturation levels, the perturbed approach can provide an improvement in out-of-band power rejection, at the cost of a small degradation in demodulation performance. Also, the design flexibility available through use of multiple linear components overcomes the rigidity inherent is use of single-linear component compander designs. The multi-component design provides compander solutions where single component solutions fail to exist due to

violation of the signal amplitude probability density function constraints. The perturbed approach thus further widens the trade space for compander design.

As a final note, the approach can be used to solve the problem of non-negativity of the p.d.f. for the full optimal solution developed and discussed in [42], by perturbing the tail of the optimal solution to meet the unity p.d.f. and constant power constraints.

APPENDIX A

From the unity c.d.f. condition on $g_\varepsilon(x)$, we have

$$\int_{a_0}^{A_C} g_\varepsilon(x)dx = 1 - \int_0^{a_0} f_R(x)dx = e^{-\frac{a_0^2}{\sigma^2}}. \tag{A.1}$$

Now from (1)

$$\int_{a_0}^{A_C} g_\varepsilon(x)dx = \int_{a_0}^{A_C} \sum_{i=0}^{N} U_i(x, \varepsilon_i, \varepsilon_{i+1})dx = \sum_{i=0}^{N} \int_{a_i}^{a_{i+1}} m_i x + b_i dx$$

where

$$m_i = \frac{(\beta_{i+1} - \beta_i) + (\varepsilon_{i+1} - \varepsilon_i)}{a_{i+1} - a_i},$$
$$b_i = \beta_i + \varepsilon_i - \frac{a_i\big[(\beta_{i+1} - \beta_i) + (\varepsilon_{i+1} - \varepsilon_i)\big]}{a_{i+1} - a_i}.$$

Thus

$$\sum_{i=0}^{N} \int_{a_i}^{a_{i+1}} m_i x + b_i dx = \sum_{i=0}^{N} m_i \left(\frac{a_{i+1}^2}{2} - \frac{a_i^2}{2}\right) + b_i(a_{i+1} - a_i)$$

which after much simplification gives

$$\int_{a_0}^{A_C} g_\varepsilon(x)dx = \sum_{i=0}^{N} T_i^1 \beta_i + T_i^2 \beta_{i+1} + \varepsilon_i \left(\frac{a_{i+1} - a_i}{2}\right) + \varepsilon_{i+1}\left(\frac{a_{i+1} - a_i}{2}\right) \tag{A.2}$$

for T_i^1 and T_i^2 defined as

$$T_i^1 = a_{i+1} - \frac{a_{i+1}^2 - a_i^2}{2(a_{i+1} - a_i)},\ T_i^2 = \frac{a_{i+1}^2 - a_i^2}{2(a_{i+1} - a_i)} - a_i.$$

Hence from (A.1) and (A.2) we get the expression in (3) for

$$\xi_i = \frac{a_{i+1} - a_i}{2},\ C_1 = e^{-\frac{a_0^2}{\sigma^2}} - \sum_{i=0}^{N} T_i^1 \beta_i + T_i^2 \beta_{i+1}.$$

APPENDIX B

From the constant power constraint on $g_\varepsilon(x)$, we have

$$\int_{a_0}^{A_C} x^2 g_\varepsilon(x)dx = \sigma^2 - \int_0^{a_0} x^2 f_R(x)dx = \left(a_0^2 + \sigma^2\right)e^{-\frac{a_0^2}{\sigma^2}}. \tag{B.1}$$

Now

$$\int_{a_0}^{A_C} x^2 g_\varepsilon(x)dx = \int_{a_0}^{A_C} x^2 \sum_{i=0}^{N} U_i(x, \varepsilon_i, \varepsilon_{i+1})dx = \sum_{i=0}^{N} \int_{a_i}^{a_{i+1}} x^2(m_i x + b_i)dx$$

which after much manipulation becomes

$$\int_{a_0}^{A_C} x^2 g_\varepsilon(x)dx = \sum_{i=0}^{N} \eta_i^1 \beta_i + \eta_i^2 \beta_{i+1} + \varepsilon_i \eta_i^1 + \varepsilon_{i+1}\eta_i^2 \tag{B.2}$$

where

$$\eta_i^1 = \frac{a_{i+1}^3 - a_i^3}{3} - \frac{a_{i+1}^4 - a_i^4}{4(a_{i+1} - a_i)} + \frac{a_i\big(a_{i+1}^3 - a_i^3\big)}{3(a_{i+1} - a_i)},$$
$$\eta_i^2 = \frac{a_{i+1}^4 - a_i^4}{4(a_{i+1} - a_i)} - \frac{a_i\big(a_{i+1}^3 - a_i^3\big)}{3(a_{i+1} - a_i)}.$$

From (B.2) using (B.1), we get (4), where

$$C_2 = \left(a_0^2 + \sigma^2\right)e^{-\frac{a_0^2}{\sigma^2}} - \sum_{i=0}^{N} \eta_i^1 \beta_i + \eta_i^2 \beta_{i+1}.$$

REFERENCES

[1] J. Zhou *et al.*, "A modified shuffled frog leaping algorithm for PAPR reduction in OFDM systems," *IEEE Trans. Broadcast.*, vol. 61, no. 4, pp. 698–709, Dec. 2015.

[2] Y.-J. Cho *et al.*, "Low-complexity PTS schemes using dominant time-domain samples in OFDM systems," *IEEE Trans. Broadcast.*, vol. 63, no. 2, pp. 440–445, Jun. 2017.

[3] H.-S. Joo, K.-H. Kim, J.-S. No, and D.-J. Shin, "New PTS schemes for PAPR reduction of OFDM signals without side information," *IEEE Trans. Broadcast.*, vol. 63, no. 3, pp. 562–570, Sep. 2017.

[4] K.-H. Kim, "On the shift value set of cyclic shifted sequences for PAPR reduction in OFDM systems," *IEEE Trans. Broadcast.*, vol. 62, no. 2, pp. 496–500, Jun. 2016.

[5] W. Wang, M. Hu, Y. Li, and H. Zhang, "A low-complexity tone injection scheme based on distortion signals for PAPR reduction in OFDM systems," *IEEE Trans. Broadcast.*, vol. 62, no. 4, pp. 948–956, Dec. 2016.

[6] J. Hou, X. Zhao, F. Gong, F. Hui, and J. Ge, "PAPR and PICR reduction of OFDM signals with clipping noise-based tone injection scheme," *IEEE Trans. Veh. Technol.*, vol. 66, no. 1, pp. 222–232, Jan. 2017.

[7] P. Yu and S. Jin, "A low complexity tone reservation scheme based on time-domain kernel matrix for PAPR reduction in OFDM systems," *IEEE Trans. Broadcast.*, vol. 61, no. 4, pp. 710–716, Dec. 2015.

[8] S. Shu, D. Qu, L. Li, and T. Jiang, "Invertible subset QC-LDPC codes for PAPR reduction of OFDM signals," *IEEE Trans. Broadcast.*, vol. 61, no. 2, pp. 290–298, Jun. 2015.

[9] S.-H. Wang, W.-L. Lin, B.-R. Huang, and C.-P. Li, "PAPR reduction in OFDM systems using active constellation extension and subcarrier grouping techniques," *IEEE Commun. Lett.*, vol. 20, no. 12, pp. 2378–2381, Dec. 2016.

[10] Y.-C. Liu, C.-F. Chang, S.-K. Lee, and M.-C. Lin, "Deliberate bit flipping with error-correction for PAPR reduction," *IEEE Trans. Broadcast.*, vol. 63, no. 1, pp. 123–133, Mar. 2017.

[11] S.-H. Wang, C.-P. Li, K.-C. Lee, and H.-J. Su, "A novel low-complexity precoded OFDM system with reduced PAPR," *IEEE Trans. Signal Process.*, vol. 63, no. 6, pp. 1366–1376, Mar. 2015.

[12] I. Sohn, "A low complexity PAPR reduction scheme for OFDM systems via neural networks," *IEEE Commun. Lett.*, vol. 18, no. 2, pp. 225–228, Feb. 2014.

[13] I. Sohn and S. C. Kim, "Neural network based simplified clipping and filtering technique for PAPR reduction of OFDM signals," *IEEE Commun. Lett.*, vol. 19, no. 8, pp. 1438–1441, Aug. 2015.

[14] K.-H. Kim, H. Park, J.-S. No, H. Chung, and D.-J. Shin, "Clipping noise cancelation for OFDM systems using reliable observations based on compressed sensing," *IEEE Trans. Broadcast.*, vol. 61, no. 1, pp. 111–118, Mar. 2015.

[15] A. Hekkala, S. Boumard, and M. Lasanen, "Exponential companding and active constellation extension comparisons for PAPR reduction," in *Proc. Int. Teletraffic Congr.*, Karlskrona, Sweden, 2014, pp. 1–5.
[16] G. S. Toor, H. Singh, and A. S. Bhandari, "PAPR reduction and BER improvement by using logrithmic companding hybrid with SLM technique in bit interleved COFDM system," in *Proc. Int. Conf Next. Gener. Inf. Technol. Summit (Confluence)*, Noida, India, 2014, pp. 604–608.
[17] T. Sravanti and N. Vasantha, "A hybrid technique to reduce PAPR in OFDM systems," in *Proc. Int. Conf. Adv. Elect. Electron. Inf. Commun. Bio Informat.*, Chennai, India, 2017, pp. 416–421.
[18] C. Kang, Y. Liu, M. Hu, and H. Zhang, "A low complexity PAPR reduction method based on FWFT and PEC for OFDM systems," *IEEE Trans. Broadcast.*, vol. 63, no. 2, pp. 416–425, Jun. 2017.
[19] J. Xiao *et al.*, "Hadamard transform combined with companding transform technique for PAPR reduction in an optical direct-detection OFDM system," *IEEE J. Opt. Commun. Netw.*, vol. 4, no. 10, pp. 709–714, Oct. 2012.
[20] B. Elmaroud, A. Faqihi, M. Abbad, and D. Aboutajdine, "PAPR reduction of FBMC signals by combining exponential companding and hadamard transforms," in *Proc. Int. Symp. Netw. Comput. Commun.*, 2014, pp. 1–4.
[21] A. S. Lakamana and A. M. Prasad, "An effective composite PAPR reduction technique of OFDM by using DFT precoding with piecewise linear companding," in *Proc. Int. Conf. Commun. Electron. Syst.*, Coimbatore, India, 2016, pp. 1–6.
[22] A. Thammana and M. K. Kasi, "Improvement measures of DHT precoded OFDM over WiMAX channels with piecewise linear companding," in *Proc. IEEE Annu. India Conf.*, Bengaluru, India, 2016, pp. 1–6.
[23] R. Ghahremani and M. G. Shayesteh, "BER performance improvement and PAPR reduction in OFDM systems based on combined DHT and μ-law companding," in *Proc. Iran. Conf. Elect. Eng.*, Tehran, Iran, 2014, pp. 1483–1487.
[24] P. Elavarasan, G. Nagarajan, and A. Narayanan, "PAPR reduction in MIMO-OFDM systems using joint channel estimation and precoding," in *Proc. Int. Conf. Adv. Commun. Control Comput. Technol.*, 2012, pp. 327–331.
[25] Y. Wang, C. Yang, and B. Ai, "Iterative companding transform and filtering for reducing PAPR of OFDM signal," *IEEE Trans. Consum. Electron.*, vol. 61, no. 2, pp. 144–150, May 2015.
[26] X. Huang, J. Lu, J. Zheng, J. Chuang, and J Gu, "Reduction of peak-to-average power ratio of ofdm signals with companding transform," *Electron. Lett.*, vol. 37, no. 8, pp. 506–507, Apr. 2001.
[27] X. Wang, T. T. Tjhung, and C. S. Ng, "Reduction of peak-to-average power ratio of OFDM system using a companding technique," *IEEE Trans. Broadcast.*, vol. 45, no. 3, pp. 303–307, Sep. 1999.
[28] T. G. Pratt, N. Jones, L. Smee, and M. Torrey, "OFDM link performance with companding for PAPR reduction in the presence of non-linear amplification," *IEEE Trans. Broadcast.*, vol. 52, no. 2, pp. 261–267, Jun. 2006.
[29] X. Wang, T. T. Tjhung, C. S. Ng, and A. A. Kassim, "On the SER analysis of A-law companded OFDM system," in *Proc. IEEE GLOBECOM*, vol. 2. San Francisco, CA, USA, 2000, pp. 756–760.
[30] X. Zhang, P. Liu, J. Liu, and S. Liu, "An advanced a-law companding algorithm in VLC-OFDM," in *Proc. IEEE Glob. Conf. Consum. Electron.*, Tokyo, Japan, 2014, pp. 721–722.
[31] N. Ali, R. Almahainy, A. Al-Shabili, N. Almoosa, and R. Abd-Alhameed, "Analysis of improved μ-law companding technique for OFDM systems," *IEEE Trans. Consum. Electron.*, vol. 63, no. 2, pp. 126–134, May 2017.
[32] Y. Wang, L.-H. Wang, J.-H. Ge, and B. Ai, "An efficient nonlinear companding transform for reducing PAPR of OFDM signals," *IEEE Trans. Broadcast.*, vol. 58, no. 4, pp. 677–684, Dec. 2012.
[33] Y. Wang, J.-H. Ge, L.-H. Wang, J. Li, and B. Ai, "Nonlinear companding transform for reduction of peak-to-average power ratio in OFDM systems," *IEEE Trans. Broadcast.*, vol. 59, no. 2, pp. 369–375, Jun. 2013.
[34] T. Jiang, W. Xiang, P. C. Richardson, D. Qu, and G. Zhu, "On the nonlinear companding transform for reduction in PAPR of MCM signals," *IEEE Trans. Wireless Commun.*, vol. 6, no. 6, pp. 2017–2021, Jun. 2007.
[35] T. Jiang, W. Yao, P. Guo, Y. Song, and D. Qu, "Two novel nonlinear companding schemes with iterative receiver to reduce PAPR in multi-carrier modulation systems," *IEEE Trans. Broadcast.*, vol. 52, no. 2, pp. 268–273, Jun. 2006.
[36] T. Jiang, Y. Yang, and Y.-H Song, "Exponential companding technique for PAPR reduction in OFDM systems," *IEEE Trans. Broadcast.*, vol. 51, no. 2, pp. 244–248, Jun. 2005.
[37] S.-S. Jeng and J.-M. Chen, "Efficient PAPR reduction in OFDM systems based on a companding technique with trapezium distribution," *IEEE Trans. Broadcast.*, vol. 57, no. 2, pp. 291–298, Jun. 2011.
[38] J. Hou, J. H. Ge, and J. Li, "Trapezoidal companding scheme for peak-to-average power ratio reduction of OFDM signals," *Electron. Lett.*, vol. 45, no. 25, pp. 1349–1351, Dec. 2009.
[39] J. Hou, J. Ge, D. Zhai, and J. Li, "Peak-to-average power ratio reduction of OFDM signals with nonlinear companding scheme," *IEEE Trans. Broadcast.*, vol. 56, no. 2, pp. 258–262, Jun. 2010.
[40] S. P. DelMarco, "General closed-form family of companders for PAPR reduction in OFDM signals using amplitude distribution modification," *IEEE Trans. Broadcast.*, vol. 60, no. 1, pp. 102–109, Mar. 2014.
[41] M. Hu, Y. Li, Y Liu, and H. Zhang, "Parameter-adjustable piecewise exponential companding scheme for peak-to-average power ratio reduction in orthogonal frequency division multiplexing systems," *IET Commun.*, vol. 8, no. 4, pp. 530–536, Mar. 2014.
[42] S. DelMarco, "A constrained optimization approach to compander design for OFDM PAPR reduction," *IEEE Trans. Broadcast.*, to be published.
[43] D. G. Luenberger and Y. Ye, *Linear and Nonlinear Programming*. New York, NY, USA: Springer, 2008.

Stephen P. DelMarco (M'91) received the Ph.D. degree in mathematics from Boston University, Boston, MA, USA, in 1985, and the B.A. and M.A. degrees in mathematics from Boston College, Boston, MA, USA, in 1981.

He joined Raytheon Co., Bedford, MA, USA, where he performed missile systems and radar signal processing simulation and performance analysis, in 1986. He joined Aware, Inc., Bedford, MA, USA, where he led various efforts in applying wavelets to signal and image processing problems, and performed research and development in biometrics, in 1992. Since joining BAE Systems, Burlington, MA, USA, in 2003, he has been performing research and development in statistical target tracking, automatic target detection and recognition, multisensor data fusion and image registration, sensor modeling, and communications signal processing.

Dr. DelMarco was a recipient of the BAE Systems Joseph G. Wohl Achievement Award for best published technical paper in 2005. He has over 40 publications in peer-reviewed journals and conferences, lightly reviewed conferences, and closed industry conferences, in applied mathematics, mathematical modeling, and signal and image processing.